We are IntechOpen,
the world's leading publisher of
Open Access books
Built by scientists, for scientists

4,800
Open access books available

122,000
International authors and editors

135M
Downloads

154
Countries delivered to

Our authors are among the
TOP 1%
most cited scientists

12.2%
Contributors from top 500 universities

WEB OF SCIENCE™
Selection of our books indexed in the Book Citation Index
in Web of Science™ Core Collection (BKCI)

Interested in publishing with us?
Contact book.department@intechopen.com

Numbers displayed above are based on latest data collected.
For more information visit www.intechopen.com

2

Ferroelectric and Multiferroic Tunnel Junctions

Tianyi Cai[1], Sheng Ju[1], Jian Wang[2] and Zhen-Ya Li[1]
[1]*Department of Physics and Jiangsu Key Laboratory of Thin Films*
Soochow University, Suzhou, 215006
[2]*Department of Teaching Affairs,*
Wuxi City College of Vocational Technology, Wuxi, 214153
China

1. Introduction

The phenomenon of electron tunneling has been known since the advent of quantum mechanics, but it continues to enrich our understanding of many fields of physics, as well as offering a route toward useful devices. A tunnel junction consists of two metal electrodes separated by a nanometer-thick insulating barrier layer, in which an electron is allowed to transverse a potential barrier exceeding the electron's energy. The electron therefore has a finite probability of being found on the opposite side of the barrier. In the 1970's, spin-dependent electron tunneling from ferromagnetic metal electrodes across an amorphous Al_2O_3 film was observed by Tedrow and Meservey(1)(2). Based on this discovery, Jullière proposed and demonstrated that in *a magnetic tunnel junction* tunnel current depends on the relative magnetization orientation of the two ferromagnetic electrodes(3). Such a phenomenon nowadays is known as *tunneling magnetoresistance*(TMR)(4). Magnetic tunnel junctions may be very useful for various technological applications in spintronics devices such as magnetic field sensors and magnetic random access memories. Other insulators are also used for tunnel barriers. For example, epitaxial perovskite $SrTiO_3$ barriers were studied by De Teresa *et al.* to demonstrate the importance of interfaces in spin-dependent tunneling(5). In tunnel junctions with MgO barriers, Ikeda *et al.* found large magnetoresitance as high as 604% at room temperature and 1144% at 5 K(6), which approaches the theoretical predictions of Butler *et al.*(7) and Mathon *et al.*(8). Despite the diversity of materials used as the barrier of the tunnel junctions, the common feature is that almost all the barriers are nonpolar dielectrics.
On the other hand, magnetic insulators, i.e, EuO, EuS and EuSe, are used for tunnel barriers. Spin filtering has been observed in these junctions as were first discussed by Moodera *et al.*(9). in 1988. They observed that the tunneling current in Au/EuS/Al junction has a spin polarization with the magnitude as high as 80%. and attributed it to the electron tunneling across the spin-dependent barriers (Fig.1). Later, they reported that the tunneling current across Ag/EuSe/Al junctions has an enhanced spin-polarization reaching 97%(10). Recently, using EuO with a higher Curier temperature (69 K) than EuS (16.7 K) and EuSe (4.6 K), Santos et al. obtained 29% spin-polarized tunneling current(11). Naturally, if electrodes are not normal metals, but ferromagnetic materials, both TMR and spin filter effects can be observed(Fig.2)(12).
Another important concept is the *ferroelectric tunnel junction* (FTJ)(13)(14)(15), which take advantage of a ferroelectric as the barrier material. Ferroelectrics possess a spontaneous

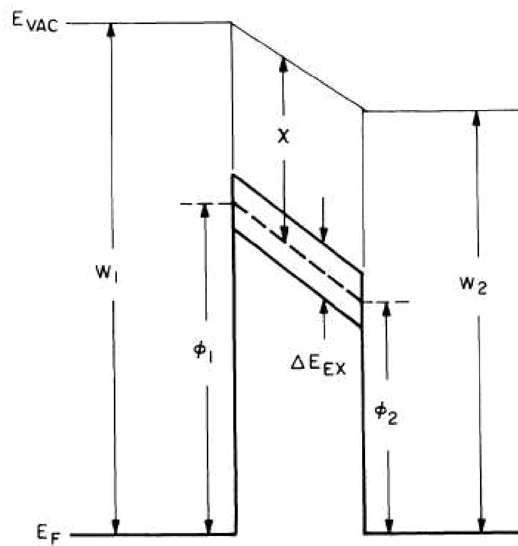

Fig. 1. Schematic illustration of tunnel barrier of a Au/EuS/Al junction. W_1 and W_2 are the work functions of Au and Al, respectively. χ is the electron affinity of EuS. The barrier heights at the Au and Al interfaces are shown as Φ_1 and Φ_2 at the bottom of the EuS conduction band (dashed line) at T>16.7 K. The bottom of the two bands shown at $T \leq T_C$ by the solid lines separated by ΔE_{ex} are the barriers seen by the two spin directions.(9)

electric polarization that can be switched by an applied electric field. This adds a new functional property to a tunnel junction. Nowadays, there are worldwide efforts to include FTJs into various nanoscale devices such as Gbit nonvolatile semiconductor memories. This

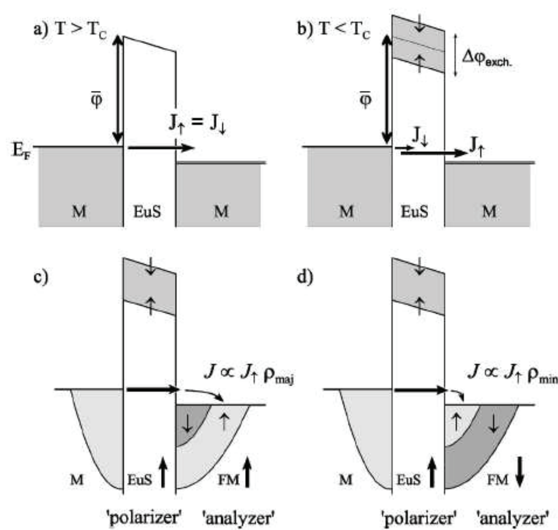

Fig. 2. Schematic illustration of spin filtering and the MR effect. (a) above T_C of the EuS filter the two spin currents are equal. (b) below the T_C of EuS, the tunnel barrier is spin split, resulting in a highly spin polarized tunnel current. With a ferromagnetic (FM) electrode, the tunnel current depends on the relative magnetization orientation. For parallel alignment (P), (c) a large current results, while for antiparallel alignment (AP), (d) a small current results.(12)

may open new exciting perspectives but also give rise to important fundamental questions. For example, *can ferroelectricity exist in a nanometer-thick barrier film?* As is well-known, ferroelectricity is a collective phenomenon (as magnetism or superconductivity) and it results from a delicate balance between long-range Coulomb forces (dipole-dipole interaction) which are responsible for the ferroelectric state and short-range repulsion which favor the paraelectric cubic state. When the size of a ferroelectric sample is reduced, both Coulomb and short-range forces are modified. This leads to a behavior at very small size that cannot be trivially predicted and causes eventually a suppression of the interesting functional properties below what is referred to the correlation volume. The ferroelectric instability of ultra-thin films and ultra-small particles has been an open question for several decades. Recently, experimental and theoretical investigations showed that ferroelectricity may persist even at a film thickness of a few unit cells under appropriate mechanical (lattice strain) and electric boundary (screening) conditions. In particular, it was discovered that, in organic ferroelectrics, ferroelectricity can be sustained in thin films of a few monolayer thickness (16). In perovskite ferroelectric oxides, ferroelectricity was observed down to a nanometer scale (17). This fact is consistent with first-principle calculations that predict a nanometer critical thickness for a FTJ (18). As a result, the existence of ferroelectricity at such a small film thickness makes it possible to use ferroelectrics as tunnel barriers.
Let us now turn to a general outline of this chapter. We will begin with a discussion of the concept of a ferroelectric tunnel junction, then show that the reversal of the electric polarization in the ferroelectric produces a change in the electrostatic potential profile across the junction. This leads to the resistance change which can reach a few orders of magnitude, namely, the giant *tunneling electroresistance* (TER) effect. Interface effect, strain effect and composite barrier are also discussed. Next, we will show that functional properties of FTJs can be extended by adding the spin degree of freedom to FTJs. This makes the junctions multiferroic (that is, simultaneously ferromagnetic and ferroelectric). The interplay between ferroelectric and magnetic properties in a multiferroic tunnel junction (MFTJ) may affect the electric polarization of the ferroelectric barrier, the electronic and magnetic properties of the interface, and the spin polarization of the tunneling current. Therefore, TMR and spin filtering effect observed in MTJs can also be observed in MFTJs. Such a new kind of tunnel junction may be very useful for future technological applications. Several ways to obtain MFTJs are introduced, such as (1) replacing one normal metal electrode with ferromagnetic one, (2) replacing ferromagnetic barriers with multiferroic materials, and (3) using a composite of ferromagnets and ferroelectrics as the barrier. These studies open an avenue for the development of novel electronic devices in which the control of magnetization can be achieved by the electric field via magnetoelectric coupling. Finally, we look at the magnetoelectric coupling effect in the ferroelectric-based junctions, which is independent of particular chemical or physical bonding.

2. Ferroelectric tunnel junction

The concept of a FTJ is illustrated in Fig.3(15), which shows the simplified band structure of a tunnel junction with a ferroelectric barrier. If the ferroelectric film is sufficiently thin but still maintains its ferroelectric properties, the surface charges in the ferroelectric are not completely screened by the adjacent metals [Fig.4(a)] and therefore the depolarizing electric field E in the ferroelectric is not zero. The electrostatic potential associated with this field depends on the direction of the electric polarization [Fig.4(b)]. If a FTJ is made of metal electrodes which have different screening lengths, this leads to the asymmetry in the potential profile for the

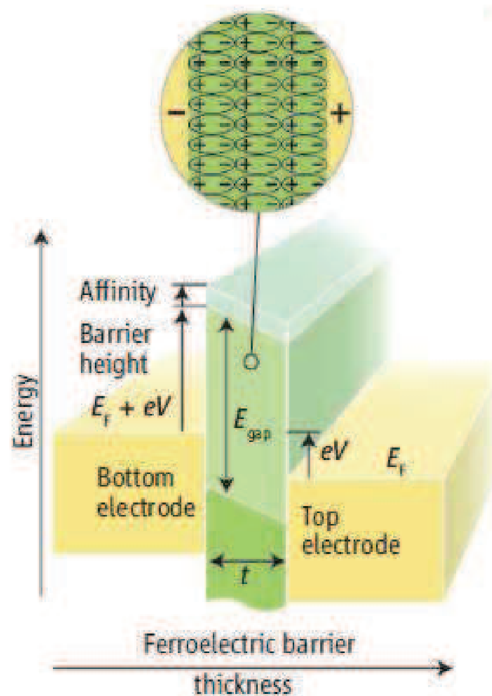

Fig. 3. (Color online). Schematic diagram of a tunnel junction, which consists of two electrodes separated by a nanometer-thick ferroelectric barrier layer(15). (E_{gap} is the energy gap. E_F is the Fermi energy, V is the applying voltage, t is the barrier thickness.)

opposite polarization directions. Thus, the potential seen by transport electrons changes with the polarization reversal which leads to the TER effect.

Electrostatic effect. The above arguments can be made quantitative by applying a Thomas-Fermi model. The screening potential within metal 1 and metal 2 electrode is given by(19)

$$\varphi(z) = \begin{cases} \frac{\sigma_S \delta_L e^{-|z|/\delta_L}}{\varepsilon_0}, & z \leq 0 \\ -\frac{\sigma_S \delta_R e^{-|z-d|/\delta_R}}{\varepsilon_0}, & z \geq d \end{cases} \tag{1}$$

Here δ_L and δ_R are the Thomas-Fermi screening lengths in the M_1 and M_2 electrodes. σ_S is the magnitude of the screening charges and can be found from the continuity of the electrostatic potential:

$$\varphi(0) - \varphi(d) = \frac{d(P - \sigma_S)}{\varepsilon_F} \tag{2}$$

Here P is considered to be the absolute value of the spontaneous polarization, and the introduction of the dielectric permittivity ε_F is required to account for the induced component of polarization resulting from the presence of an electric field in the ferroelectric. Using Eqs.(1)-(2) and introducing the dielectric constant $\varepsilon = \varepsilon_F/\varepsilon_0$, σ_S can be expressed as $\sigma_S = dP/[\varepsilon(\delta_L + \delta_R) + d]$.

Figure 4(b) shows the electrostatic potential in a M_1-FE-M_2 junction assuming that metals M_1 and M_2 have different screening lengths, such that $\delta_L > \delta_R$. It follows from Eq.(1) that different screening lengths result in different absolute values of the electrostatic potential at the interfaces, so that $\varphi_1 \equiv |\varphi(0)| \neq \varphi_2 \equiv |\varphi(d)|$, which makes the potential profile highly asymmetric. The switching of the polarization in the ferroelectric layer leads to the change in the potential which transforms to the one shown in Fig.4(b) by the dashed line, thus, inevitably leading to the change in the resistance of the junction.

Tunneling electroresistance effect. If the thickness of the ferroelectric barrier is so small that the dominant transport mechanism across the FTJ is the direct quantum-mechanical electron tunneling. The conductance of FTJ can be calculated, for example, at a small applied bias voltage the conductance of a tunnel junction per area A is(20)

$$\frac{G}{A} = \frac{2e^2}{h} \int \frac{d^2 k_\parallel}{(2\pi)^2} T\left(E_F, k_\parallel\right) \tag{3}$$

Here, T is the transmission coefficient evaluated at the Fermi energy E_F for a given value of the transverse wave vector $k_\parallel$, which can be obtained from the Schrödinger equation for an electron moving in the potential.
The overall potential profile seen by the transport electrons is a superposition of the electrostatic potential shown in Fig.4(b), the electronic potential which determines the bottom of the bands in the two electrodes with respect to the Fermi energy E_F, and the potential barrier created by the ferroelectric insulator. The resulting potential for the two opposite orientations of polarization in the ferroelectric barrier is shown schematically in Fig.5 for

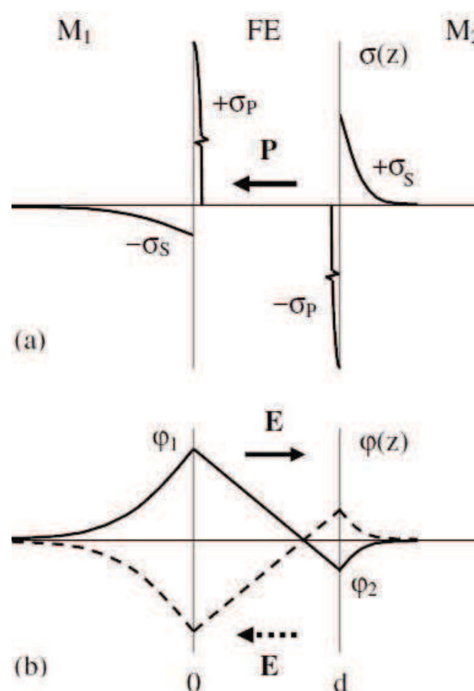

Fig. 4. Electrostatics of a M_1-FE-M_2 junction: (a) charge distribution and (b) the respective electrostatic potential profile (solid line)(14). The polarization P creates surface charge densities, $\pm\sigma_P = \pm|P|$, on the two surfaces of the ferroelectric film. These polarization charges $\pm\sigma_P$, are screened by the screening charge per unit area, $\mp\sigma_S$, which is induced in the two metal electrodes. It is assumed that metal 1 (M_1) and metal 2 (M_2) electrodes have different screening lengths ($\delta_L > \delta_R$) which lead to the asymmetry in the potential profile. The dashed line in (b) shows the potential when the polarization P in the ferroelectric is switched, resulting in the reversal of the depolarizing field E. The following assumptions are made: (1) The ferroelectric is assumed to be uniformly polarized in the direction perpendicular to the plane. (2) The ferroelectric is assumed perfectly insulating so that all the compensating charges resides in the electrodes. (3) The short-circuited FTJs are discussed.

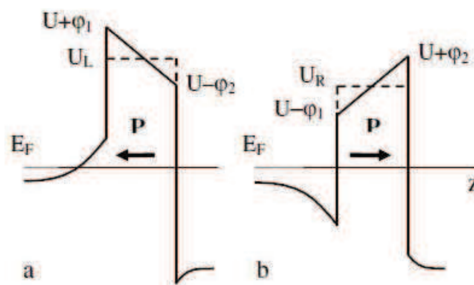

Fig. 5. Schematic representation of the potential profile $V(z)$ in a M_1-FE-M_2 junction for polarization pointing to the left (a) and for polarization pointing to the right (b), assuming that $\delta_1 > \delta_2$. The dashed lines show the average potential seen by transport electrons tunneling across the ferroelectric barrier(14). The horizontal solid line denotes the Fermi energy, E_F.

$\delta_L > \delta_R$. Indeed, the average potential barrier height seen by the transport electrons travelling across the ferroelectric layer for polarization pointing to the left, $U_L = U + (\varphi_1 - \varphi_2)/2$, is not equal to the average potential barrier height for polarization pointing to the right, $U_R = U + (\varphi_1 - \varphi_2)/2$, as is seen from Figs. 5(a) and 5(b). This make the conductance G_L for polarization pointing to the left much smaller than the conductance G_R for polarization pointing to the right (Fig.6(a)), thereby resulting in the TER effect(Fig. 6(b))(14).
Experimentally, ferroelectric tunnel junctions with different ferroelectric barriers have been fabricated successfully and giant tunneling electroresistance effects have been observed. Garcia et al.(21) and Gruverman et al.(22) reported that giant TER effects reached 75000% through 3 nm-thick $BaTiO_3$ barrier at room temperature. Crassous et al. observed that the TER reached values of 50000% through a 3.6 nm $PbTiO_3$(23). Maksymovych et al. found

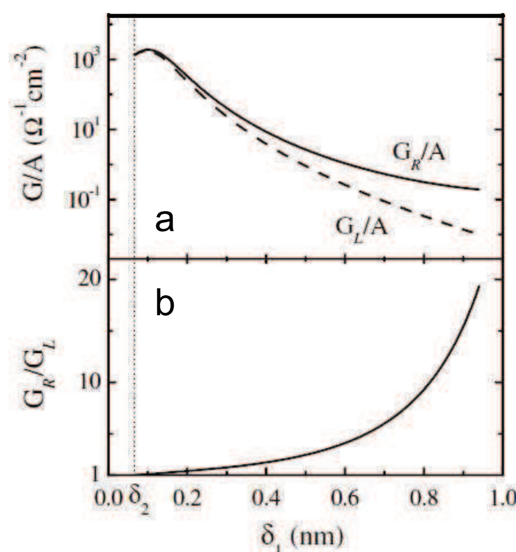

Fig. 6. (a) conductance per unit area for polarization oriented to the right, G_R/A (solid line) and for polarization oriented to the left, G_L/A (dashed line); (b) conductance change, $G_R = G_L$, associated with the polarization switching in the ferroelectric barrier (14). The vertical dotted line indicates the value of $\delta_1 = \delta_2$ at which no asymmetry in the potential profile and, hence, no conductance difference is predicted.

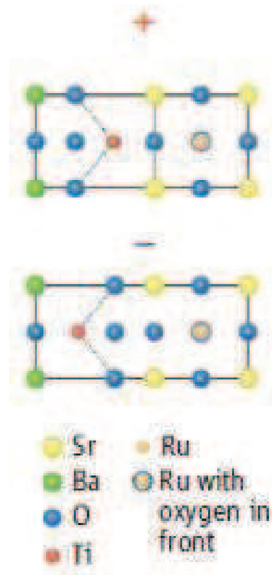

Fig. 7. Interface effect of a FTJ (15).

that the large spontaneous polarization of the $Pb(Zr_{0.2}Ti_{0.8})O_3$ film resulted in up to 500-fold amplification of the tunneling current upon ferroelectric switching(24).

Interface and strain effect. Interestingly, recent experimental(25) and theoretical(26) studies indicate that ionic displacements within the electrodes, in a few atomic monolayers adjacent to the ferroelectric, may affect the electron screening. The polarization switching alters positions of ions at the interfaces that influences the atomic orbital hybridizations at the interface and hence the transmission probability (see Fig.7). On the other hand, the piezoelectricity of a ferroelectric barrier under an applied voltage produces a strain (see Fig.8) that changes transport characteristic of the barrier such as the barrier width and the attenuation constant(27).

FTJs with ferroelectric/dielectric composite barriers. It is an efficient way to enhance the TER by using a layered composite barrier combing a functional ferroelectric film (FE) and a thin film of a nonpolar dielectric material (DI)(28). Due to the change in the electrostatic potential

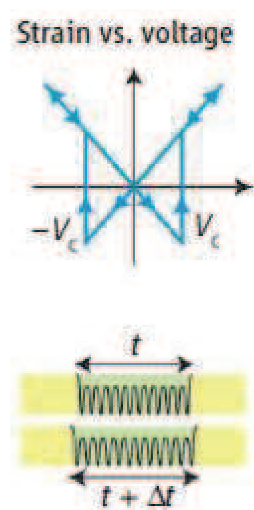

Fig. 8. Strain effect of a FTJ (15).

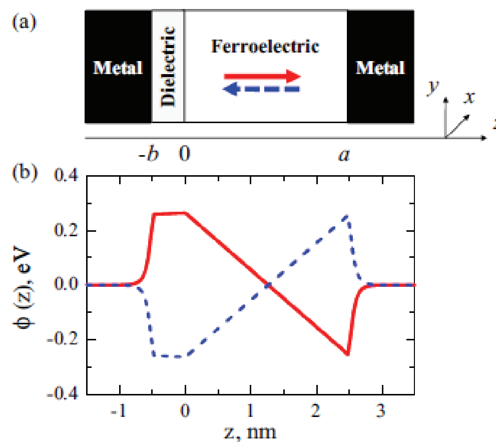

Fig. 9. (Color online) Geometry (a) and the electrostatic potential profile for the two opposite polarization orientations (b) of a FTJ: a=25 Å, b=5 Å, ε_d=300, ε_f =90, δ =1 Å, and P=20 $\mu C/cm^2$(28).

induced by polarization reversal, the nonpolar dielectric film adjacent to one of the interfaces acts as a switching changing its barrier height from a low to high value (Fig.9), resulting in a dramatic change in the transmission across the FTJ. The predicted values of TER are giant, indicating that the resistance ratio between the two polarization-orientation states in such FTJs may reach hundred thousands and even higher as shown in Fig.10. Furthermore, Wu et al. proposed that if the interface between the FE and the dielectric layer is very sharp and space charges exist at this interface, the TER will be enhanced strongly(29).

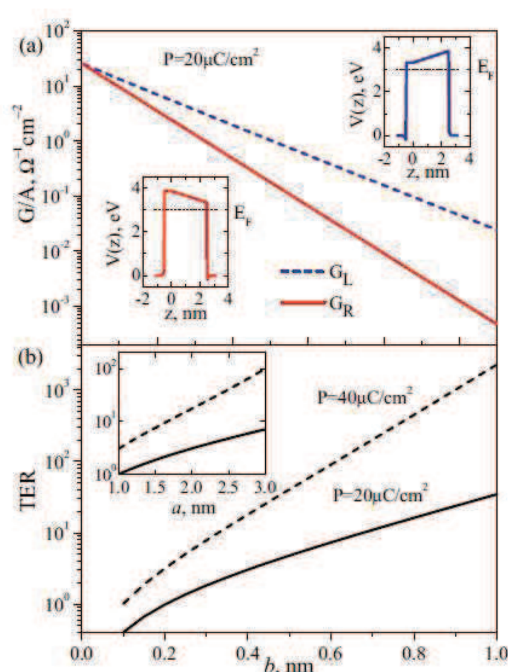

Fig. 10. (Color online) (a) Conductance of a FTJ for two opposite polarization orientations: Left (solid line) and right (dashed line), as a function of dielectric layer thickness. The insets show the corresponding tunneling barrier profiles. (b) TER as the function of dielectric layer thickness for two polarizations P=20 $\mu C/cm^2$ (solid line) and P=40 $\mu C/cm^2$ (dashed line). The inset shows TER as the function of the ferroelectric film thickness. U_d=0.6 eV, ε_d=300(28).

It should be noted that FTJs with composite barriers (M/FE/DI/M) does not require different electrodes. This may be more practical for device application than the conventional FTJs (M_1/FE/M_2). For FTJs as M_1/FE/M_2, asymmetry is necessary for the TER effect, which may be intrinsic (e.g., due to nonequivalent interfaces) or intentionally introduced in the system (e.g., by using different electrodes).

3. Multiferroic tunnel junctions (MFTJ)

A MFTJ is simultaneously ferromagnetic and ferroelectric. The transport behaviors of MFTJs can be controlled by the magnetic and electric field. Furthermore, the interplay between ferromagnetic and ferroelectric properties may affect the electric polarization of the ferroelectric barrier, the electronic and magnetic properties of the interface, and the spin polarization of the tunneling current. This indicates that not only TER effect, TMR and spin filtering effects may also be observed in MFTJs.

3.1 Ferromagnet/ferroelectric/normal metal junctions

By replacing normal metal electrode with a highly spin-polarized (ferromagnetic) material, such as diluted magnetic semiconductor(30), doped manganite(31), double perovskite manganites, CrO_2 and Heussler alloys, spin degrees of freedom can be incorporated into existing FTJs. In such MFTJs, the spin-polarized electrons from a ferromagnetic metallic electrode tunnel through a ferroelectric thin film which serves tunneling barrier. The reversal of the electric polarization of the ferroelectric film leads to a sizable change in the spin polarization of the tunneling current. This provides a two-state electric control of the spin polarization, including the possibility of switching from zero to nonzero or from negative to positive spin polarization and vice versa.

Electrostaticeffect. As is discussed on FTJs, the switching of the electric polarization changes the potential profile of the whole junction. Then, how does this change affect the conductance of the minority- and majority-spin carriers? As shown in Fig.11, for the electric polarization of the FE barrier pointing to the left (i.e., towards the FM electrode), majority-spin carriers experience an additional barrier compared to minority-spin carriers [compare the solid and dashed lines in Fig. 11(a)], since the spin dependent potential in FM electrode is $V_1^{\sigma} = V_1 \pm 1/2\Delta_{ex}$, σ is the spin index $\sigma =\downarrow,\uparrow$, Δ_{ex} is the exchange splitting strength. This occurs if the magnitude of the electrostatic potential at the FM/FE interface, $\varphi_1 \equiv \varphi(0)$, is larger than the Fermi energy with respect to the bottom of the minority-spin band, i.e., $E_F - V_1^{\downarrow} - \varphi_1 < 0$. If this condition is met, the spin polarization of the tunneling current is positive and weakly dependent on the potential barrier height. On the other hand, for the electric polarization pointing to the right (Fig. 11(b)), i.e., towards the NM electrode, the tunneling barrier is the same for majority and minority spins [compare the solid and dashed lines in Fig. 11(b)]. In this case, the magnitude of the spin polarization of the tunneling current is largely controlled by the exchange splitting of the bands and the potential profile across the structure. When $E_F - V_1^{\downarrow} - \varphi_1 > 0$, the asymmetry between R and L is due to the different barrier transparencies as a result of the different band structures of the two electrodes. Thus, by reversing the electric polarization of the FE barrier it is possible to switch the spin polarization of the injected carriers between two different values, thereby providing a two-state spin-polarization control of the device.

Spin filtering effect. The spin polarization of the conductance can be defined by $\Pi = G_{\uparrow} - G_{\downarrow}/G_{\uparrow} + G_{\downarrow}$, where the conductance can be calculated from Eq. (3). Figs. 12(a) and

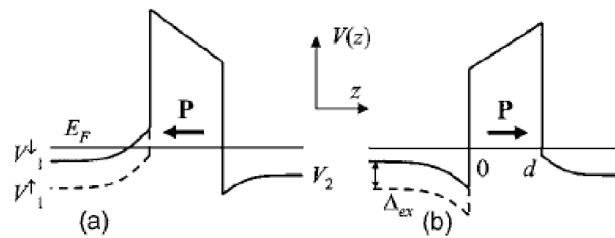

Fig. 11. (Color online) (a) Conductance of a FTJ for two opposite polarization orientations: Left (solid line) and right (dashed line), as a function of dielectric layer thickness(30). The insets show the corresponding tunneling barrier profiles. (b) TER as the function of dielectric layer thickness for two polarizations P=20 $\mu C/cm^2$ (solid line) and P=40 $\mu C/cm^2$ (dashed line). The inset shows TER as the function of the ferroelectric film thickness. U_d=0.6 eV, ε_d=300.

12(b) show the calculated conductance and spin polarization of the conductance as a function of the potential barrier height, U, in the ferroelectric barrier. It is seen that, for P pointing towards the ferromagnetic electrode, the spin polarization, Π_L, is positive and is weakly dependent on U, reflecting an additional tunneling barrier for minority spins (Fig. 11(a)). On the other hand, for the P pointing towards the NM electrode, the spin polarization, Π_R, is slightly negative at not too large values of U and becomes positive when U is larger than a certain value. The latter result can be understood in terms of spin-dependent tunneling across a rectangular barrier. Thus, using an appropriate FE barrier, it is possible to change the spin polarization of injected carriers from positive to negative and vice versa by reversing the electric polarization of the FE barrier. The degree of the spin polarization change in response to the electric polarization reversal depends on the carrier density in the semiconductors. This is illustrated in Fig. 12(c), which shows the dependence of the Π_L and Π_R on the Fermi energy with respect to the bottom of the minority-spin band in the FM electrode. When $E_F \leq V_1^{\downarrow}$ the DMS is fully spin polarized and hence Π_L=Π_R=1. With increasing the carrier concentration

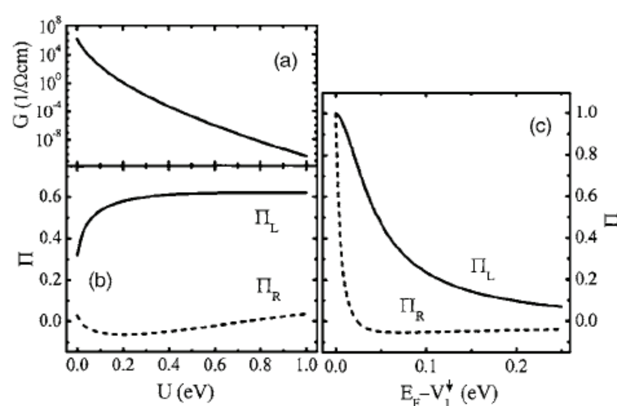

Fig. 12. (Color online)Total conductance, $G = G_{\uparrow} + G_{\downarrow}$ (a) and spin polarization (b,c) of injected current in a FM/FE/NM tunnel junction as a function of potential barrier height (a,b) and the Fermi energy (c) for the polarization of the ferroelectric barrier pointing to the left (solid lines) and pointing to the right (dashed lines) for d=3 nm. In (a) and (b) E_F-$V_1^{\uparrow}$=0.06 eV and $V_1 = V_2$; in (c) U=0.5 eV and $V_2 - V_1^{\uparrow}$=0.025 eV(30).

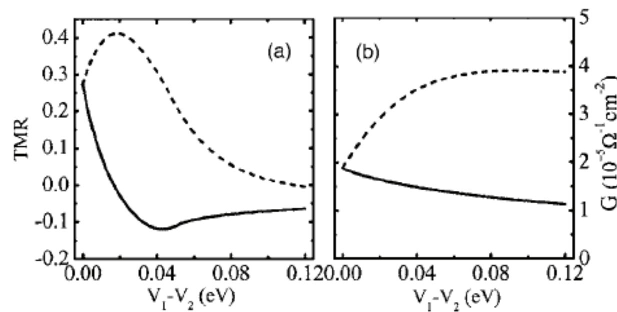

Fig. 13. (Color online) Tunneling magnetoresistance (a) and conductance, G, for parallel magnetization of the electrodes (b) in a FM/FE/FM tunnel junction versus potential difference in the two magnetic semiconductors for the electric polarization of the ferroelectric barrier pointing to the left (solid lines) and pointing to the right (dashed lines) for d=3 nm and U=0.5 eV(30).

and hence E_F, the spin polarization drops down much faster for the P pointing to the right than for the P pointing to the left, resulting in a sizable difference in the spin polarizations Π_R and Π_L. Therefore, by changing the density of carriers in the semiconductors it is possible to tune values of the spin polarization for a two-state control of the electronic device.

TMR effect. Such multiferroic tunnel junctions (MFTJ) have not yet been realized experimentally but might be promising in providing an additional degree of freedom in controlling TMR. Fig. 13(a) shows the calculated TMR in a tunnel junction with two FM electrodes separated by a FE barrier. The TMR ratio was defined by TMR = $G_P - G_{AP}/G_{AP}$, where G_P and G_{AP} are the conductances for the parallel and antiparallel magnetization, respectively. As is seen from Fig. 13(a), for $V_1 = V_2$ the TMR is independent of the orientation of P. The increasing potential difference in the two FM electrodes results in the enhancement of TMR for the P pointing to the right, whereas for the P pointing to the left the TMR drops down and becomes negative. At these conditions the MFTJ works as a device which allows switching the TMR between positive and negative values. As follows from Fig. 13(b), there is a sizable difference in the overall conductance of the junction for the two orientations of polarization, namely, the TER effect. Therefore, there is a coexistence of TMR and TER effects in such MFTJs.

3.2 MFTJs with a single-phase multiferroic barrier

Another type of MFTJ is feasible in which the barrier itself is made of a material that exhibits MF properties in the bulk, such as $BiFeO_3$ and $BiMnO_3$. In multiferroic materials, the coexistence of ferroelectric and ferromagnetic orders will provide a unique opportunity for encoding information independently in electric polarization and magnetization. Consequently, it will open new applications of multiferroic tunnel junctions on logic programming. Nowadays, several multiferroic tunneling junctions have been successfully fabricated. For example, Gajek et al. showed that $BiMnO_3$ tunnel barriers may serve as spin filters in magnetic tunnel junctions(32). This work was further advanced to demonstrate the presence of ferroelectricity in ultrathin $BiFeO_3$ films grown epitaxially on a half-metallic $La_{2/3}Sr_{1/3}MnO_3$ electrode(33)(34) and $La_{0.1}Bi_{0.9}MnO_3$(35).

In this section, two kinds of single-phase MFTJs will be discussed. One is normal metal/multiferroic/ferromagnetic metal (NM/MF/FM) junction(36). The other is FM_1/MF/FM_2 junctions(37), in which both electrodes and the barrier are ferromagnetic. TMR

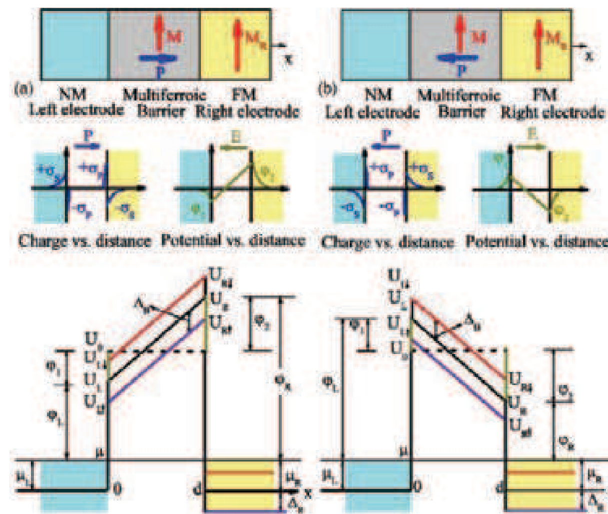

Fig. 14. (Color online) Schematic illustration of our multiferroic spin-filter tunneling junction, the charge distribution and corresponding electrostatic potential, and the overall potential profile (from top to bottom)(36). A NM electrode is placed in the left half-space $z < 0$, a multiferroic barrier of thickness t, and a semifinite FM electrode placed in the the right half-space $z > d$. m_L, m_B, and m_R are the effective masses in three regions. μ_L and μ_R are the Fermi energies of the left and right electrodes, respectively. Δ_R and Δ_B represent the exchange splitting of the spin-up and spin-down bands in FM electrode and the multiferroic barrier, respectively. φ_L and φ_R are, respectively, the electrostatic potentials at two interfaces relative to the Fermi level μ of the system.(a) The electric polarization P points to the right (positive). (b) P points to the left (negative). Here, it is assumed that two electrodes have different screening lengths and $\delta_1 < \delta_2$.

and spin filtering effects in these MFTJs are discussed. We also introduce the progress of the theoretical studies on these single-phase MFTJs.

Structure of NM/MF/FM Junctions. A NM/MF/FM MFTJ is illustrated in Fig.14. Similar to a FTJ, the screening potential $\varphi(z)$ of a MFTJ is $\sigma_S \delta_L e^{-|x|/\delta_L}/\varepsilon_L$ $(x \leq 0)$, and $-\sigma_S \delta_R e^{-|z-t|/\delta_R}/\varepsilon_R$ $(x \geq d)$. Here, δ_L and δ_R are the Thomas-Fermi screening lengths in the NM and FM electrodes, respectively. ε_L and ε_R are the dielectric permittivities of the NM and FM electrodes. The screening charge σ_S can be found from the continuity of the electrostatic potential: $\sigma_S = (dP/\varepsilon_B)/(\delta_L/\varepsilon_L + \delta_R/\varepsilon_R + d/\varepsilon_B)$ and ε_B is the dielectric permittivity of the tunneling barrier. The overall potential profile is asymmetric, as shown in Fig.14, because it is the sum of the electrostatic potential $\varphi(x)$, the electronic potential in the electrodes, and the rectangular potential profile U_0. Under the applied bias voltage V, the difference of the interfacial barrier heights is $\delta U = U_L - U_R = \delta\varphi + eV$, where $U_L = \mu + \varphi_L$ and $U_R = \mu + \varphi_R - eV$.

TMR and Spin filtering effects in NM/MF/FM Junctions. The model Hamiltonian for such MFTJs can be given by

$$\hat{H}_\sigma = -\left(\hbar^2/2m_v\right)\nabla^2 + U(z) - \sigma_v \Delta_v, \tag{4}$$

with the z-dependent potential $U(z) = 0$ when $z \leq 0$, $U(z) = U_L - (\delta U/d)z$ when $0 \leq x \leq d$, and $U(z) = \delta\mu - eV$ when $z > d$, and the spin indice is $\sigma_v = \theta_v \sigma$, where σ is the conserved spin orientation in three regions and v indicates L, B, or R. $\sigma = +1(\uparrow)$ or $-1(\downarrow)$ means up spin or down spin with respect to z. $\theta_v = +1(\Uparrow)$ or $-1(\Downarrow)$ denotes the magnetization orientation in the region v, parallel or antiparallel to the positive z direction. Then, $\sigma_v = +1(\uparrow)$ or $-1(\downarrow)$ is

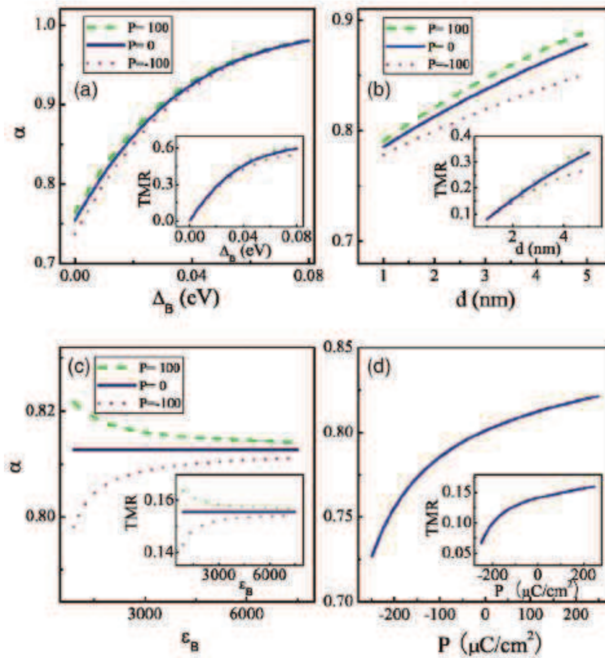

Fig. 15. (Color online) (a) The exchange splitting dependence of spin-filtering efficiency with B=1000 and d=2 nm. (b) Dielectric constant dependence of spin-filtering efficiency with Δ_B=0.01 eV and d=2 nm. (c) The thickness dependence of spin-filtering efficiency of the barrier with B=1000 and Δ_B=0.01 eV. (d) The P dependence of spin-filtering efficiency with ε_B=1000, Δ_B=0.01 eV, and d=2 nm(36). In the calculation, we set δ_L=0.07 nm, δ_R=0.08 nm, Δ_R=0.09 eV, E_F=0.1 eV, m_L=m_R =0.9m_e, m_B=1.1m_e, and U_0=0.5 eV.

the relative spin orientation, parallel or antiparallel to the given magnetization in the v region. Without loss of generality, we fix $\theta_B = +1(\Uparrow)$ and let θ_R vary. If the eigenenergy E and the transverse momentum q are conserved in this structure, the asymptotic expansion of Airys functions gives a good approximation for the transmission coefficient of each spin channel σ under a certain magnetization $\theta_R = \Uparrow or \Downarrow$(38),

$$T_{\sigma}^{\Uparrow\theta_R}(E,q) = \frac{16k_L k_{R\sigma_B}\kappa_{L\sigma_B}\kappa_{R\sigma_B}e^{-2\xi_{\sigma_B}d}}{\left(k_L^2+\kappa_{L\sigma_B}^2\right)\left(k_{R\sigma_R}^2+\kappa_{R\sigma_B}^2\right)} \tag{5}$$

where the reduced wave vectors are $k_L = \lambda_L/(E_L)^{1/2}$, $k_{R\sigma_R} = \lambda_R(E_R - \delta\mu + eV + \sigma_R\Delta_R)^{1/2}$,$\kappa_{L\sigma_B} = \lambda_B(U_{L\sigma_B} - E_B)^{1/2}$, and $\kappa_{R\sigma_B} = \lambda_B(U_{R\sigma_B} - E_B)^{1/2}$, and ξ is the decaying WKB wave vector. Here, $\lambda_v = \sqrt{2m_e^2/m_v\hbar^2}$ (v=L,B or R) with m_e the free-electron mass. When the applied bias voltage V is small and the barrier width t is large, the transmission at the Fermi level μ with $q = 0$ contributes predominantly. The zero-temperature conductance can be obtained as

$$G_{\sigma}^{\Uparrow\theta_R} = \frac{e^2}{8\pi^2\hbar}\frac{\xi_{\sigma_B}}{d}T_{\sigma}^{\Uparrow\theta_R}(\mu,0) \tag{6}$$

For a certain magnetization configuration, the total conductance is given by the sum of two channels (up spin and down spin): $G^{\Uparrow R} = G_{\uparrow}^{\Uparrow R} + G_{\downarrow}^{\Uparrow R}$. The TMR ratio is defined as TMR=$1 - G^{\Uparrow\Downarrow}/G^{\Uparrow\Uparrow}$. To show the spin-filtering effect, two sub-TMR ratio are defined as TMR$_\sigma = 1 - G^{\Uparrow\Downarrow_\sigma}/G_{\sigma}^{\Uparrow\Uparrow}$, corresponding to the higher barrier ($\sigma =\downarrow$) and lower barrier ($\sigma =\uparrow$),

respectively. Thus, a ratio can be defined as $\alpha = G_{\uparrow}^{\Uparrow\Uparrow}/(G_{\uparrow}^{\Uparrow\Uparrow} + G_{\downarrow}^{\Uparrow\Uparrow})$ to represent the ratio between conductances through the higher and lower barriers. The TMR can be reformulated as TMR=$\alpha\times$ TMR$_{\uparrow}$+(1-α)TMR$_{\downarrow}$. Clearly, when the spin-filtering effect is very strong, $\alpha \rightarrow$1(0), then TMR$\approx$TMR$_{\uparrow}$ (TMR$_{\downarrow}$), which means that tunneling electrons are fully spin polarized and TMR is dominated by one of the spin channels. The sub-TMRs can be written as

$$\mathrm{TMR}_{\sigma} = \frac{k_{R\sigma} - k_{R\bar{\sigma}}}{k_{R\sigma}} \frac{\kappa_{R\sigma}^2 - k_{R\sigma}k_{R\bar{\sigma}}}{\kappa_{R\sigma}^2 + k_{R\bar{\sigma}}^2} \tag{7}$$

where $\bar{\sigma} = -\sigma$. If spin-filtering effect is very strong, TMR$\approx$ TMR$_{\uparrow} = P_{R\uparrow}P_{B\uparrow}$, where $P_{R\uparrow} = (k_{R\uparrow} - k_{R\downarrow})/k_{R\uparrow}$ and $P_{B\uparrow} = (\kappa_{R\uparrow}^2 - k_{R\uparrow}k_{R\downarrow})/(\kappa_{R\uparrow}^2 + k_{R\downarrow}^2)$ are effective spin polarization, respectively. Because of the positive $P_{R\uparrow}$, the sign of TMR is dominated by the term in $P_{B\uparrow}$,

$$\kappa_{R\sigma}^2 - k_{R\sigma}k_{R\bar{\sigma}} \approx \lambda_B\left(\varphi_{R\uparrow} - eV\right) - \lambda_R\sqrt{(\mu_R + eV)^2 - \Delta_R^2} \tag{8}$$

which is related with the barrier height $\varphi_{R\uparrow}$ induced by electric polarization. Figs. 15 and 16 shows the effect of the barrier's properties on the spin filtering coefficient and TMR ratio.

Four Logic states. As displayed in Fig. 17 (upper panel), there are overall eight resistive states with four independent pairs (A, A'; B, B'; C, C'; and D, D'), depending on the relative orientation of neighboring magnetizations and the sign of P. Because of the magnetoelectric coupling in the multiferroics, the P and the M can be reversed by an electric field separately or simultaneously. Thus, electric-field controlled functionality can be realized, including normal electroresistance (the transition from A to B or the transition from C to D) and more significant change in resistance, i.e., electromagnetoresistance (the transition from A to D). The difference between these states is complex but important for practical application. In the lower panel of Fig. 17, we show the resistance (normalized to its value at P_c) as a function of electric polarization, and the inset displays the exchange splitting dependence of P_c, where states B and C cross. Compared with conventional TMR elements which have been applied in magnetic random access memory, and also with FTJs, the present multiferroic structure possesses both electric controllable switching and large contrast between resistive states.

TMR effect in FM$_1$/MF/FM$_2$ junctions. In the following sections, another kind of MFTJs is discussed. As shown in Fig. 18, a multiferroic barrier is separated by **two ferromagnetic** metallic electrodes, for example, half-metallic $La_{2/3}Sr_{1/3}MnO_3$ and ferromagnetic metal Co(33)(34). Evidently, it is also a kind of magnetic tunnel junction, which will show

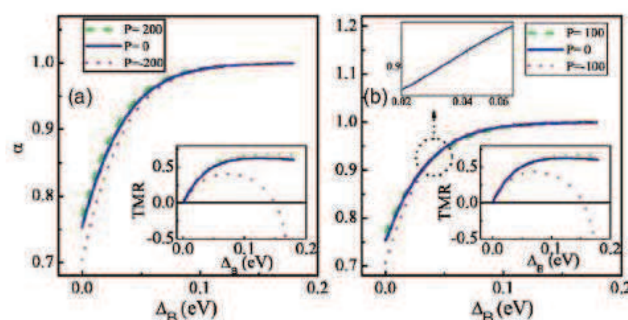

Fig. 16. (Color online) (a) The exchange splitting dependence of spin filtering efficiency for different P. δ_L=0.07 nm and δ_R =0.08 nm. The inset shows the corresponding TMR. (b) The same with (a) but with a stronger contrast between δ: δ_L=0.07 nm and δ_R=1 nm(36).

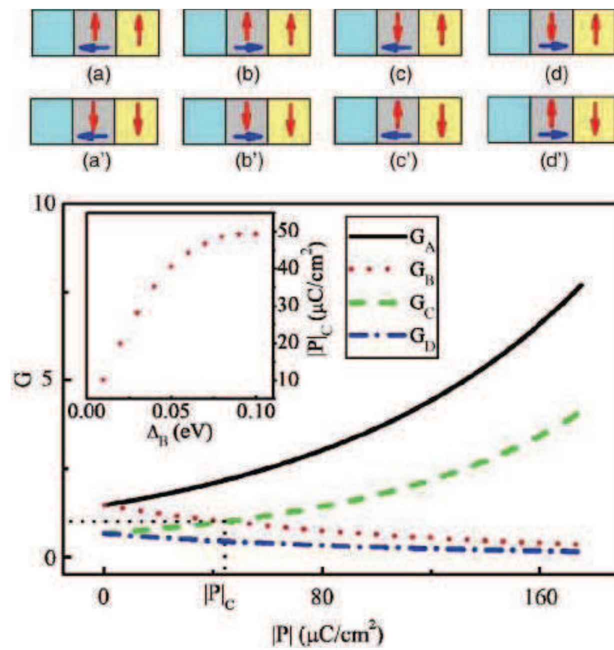

Fig. 17. (Color online) (Upper panel) Schematic illustration of multiple resistive states, depending on the orientation of P, M and MR. (Lower panel) The electric polarization dependence of normalized conductance for the four resistive states. δ_L=0.07 nm, δ_R =1 nm, ε_B=2000, and Δ_B=0.06 eV. The inset shows the Δ_B dependence of P_c(36).

significant TMR behaviors. Two theoretical models have been proposed to explain TMR effects in MTJs. One is Jullieres formula with TMR = $\frac{2P^2}{1+P^2}$(3), where the spin polarization

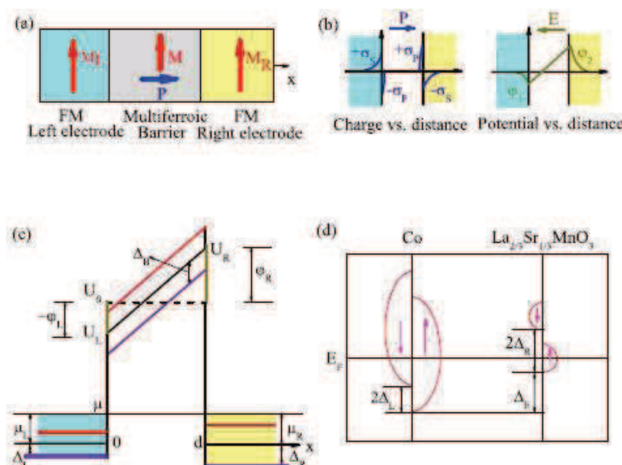

Fig. 18. (Color online) (a) Schematic illustration of MF tunnel junction. (b) Charge distribution and corresponding electrostatic potential. (c) The overall potential profile. (d) Schematic band structures of Co and half-metallic $La_{2/3}Sr_{1/3}MnO_3$(37). The exchange splittings are Δ_L, Δ_R, and Δ_B, respectively, for the left and right FM electrodes and the MF barrier. The electric polarization P induces surface charge densities, $\pm\sigma_P = \pm|P \cdot x| = P\cos\alpha$, on the two surfaces of the barrier, where α is the relative orientation between the electric polarization P and the x axis. $\theta_R = +1(\Uparrow)$ is fixed, while let θ_B and θ_L vary.

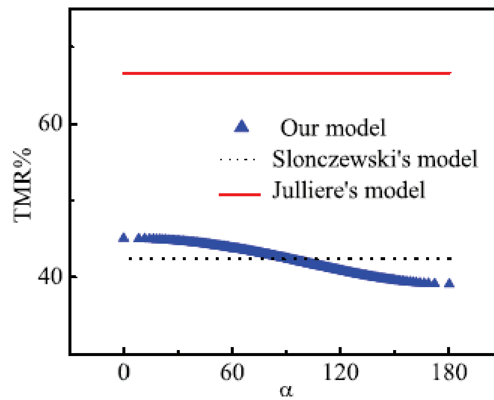

Fig. 19. (Color online) The electric polarization orientation (α) dependence of the TMR from Eq. (22)(37). The TMR from both Jullieres and Slonczewskis models is α independent. The parameters used are the same as that used in the calculations in Fig. 20. Here a 5 nm thick nonmagnetic barrier is adopted.

$P = (N_\uparrow - N_\downarrow)/(N_\uparrow + N_\downarrow)$ and N is the density of states at Fermi level. On the other hand, in the model by Slonczewski(39), the barrier height on the tunneling is considered and $P = [(k_\uparrow - k_\downarrow)/(k_\uparrow + k_\downarrow)][(\kappa^2 - k_\uparrow k_\downarrow)/(\kappa^2 + k_\uparrow k_\downarrow)]$, where $\kappa = \sqrt{(2m/\hbar^2)/(U - E_F)}$ and U is the height of barrier. However, in both models of Julliere and Slonczewski, neither the electric polarization nor the magnetism of the barrier was considered. For MFTJs, Ju *et al.* extended the previous TMR models and firstly pointed out the TMR is a function of the orientation of the electric polarization (Fig. 19). They also proved that Slonczewskis model is actually a special case of their model with P=0 (or α =0) and $\Delta_B = 0$. Their calculations show that the TMR of MFTJs are strongly influenced by the orientation of the electric polarization and the barrier properties, i.e., effective barrier height $\bar{U}$; the exchange splitting of the barrier, Δ_B; and the electric polarization in the barrier, P, which is shown in Fig.19 and Fig.20.

Tunneling electroresistance effect (TER). Since both electrodes and barrier are ferromagnetic, such tunnel electroresistance (TER), $TER = G(\pi)/G(\alpha = 0)$, is a little different from that in FTJs. In Fig. 20(e), we show such TER as for junctions with various barrier thicknesses. It is found that TER increases with the increase of d and when the magnetization of the barrier is parallel to the magnetization of right electrode, the presence of weak ferromagnetism in $BiFeO_3$ will make TER more significant (Fig. 20(f)). However, it is also noted that TER is almost independent of the magnetic configuration of two electrodes, i.e., parallel or antiparallel. These TER effects will be studied experimentally by Bea *et al.*(33)(34).

Converse piezoelectric effect. Converse piezoelectric effect may also have an important influence on the tunneling across a multiferroic(40). When the junction is applied with a bias voltage V, the converse piezoelectric property causes the strain in the barrier, which hence induces changes in the barrier thickness d, electron effective mass m_B, and position of the conduction band edge E_c. There are (27)

$$\begin{aligned} d &= d^0 + d_{33}V \\ m_B &= m_B^0(1 + \mu_{33}\Delta S_3) \\ E_C &= E_C^0 + \kappa_3 \Delta S_3 \end{aligned} \tag{9}$$

where $\Delta S_3 = d_{33}V/d^0$ is the lattice strain and d_{33}, μ_{33}, and κ_3 are, respectively, the out-of-plane piezoelectric coefficient, strain sensitivity of the effective mass, and relevant deformation potential of the conduction band in the barrier. d^0, m_B^0 , and E_c^0 are their values at $V = 0$.

If the applied voltage is positive, the barrier thickness d will be compressed and both the electron effective mass m_B and barrier height U will increase. Obviously, each of these strain-induced changes will change the electron tunneling probabilities, and therefore the spin filtering efficiency and TMR ratio (Figs. 21-22).

4. MFTJs with ferromagnet/ferroelectric composite barriers

For practical applications, the single-phase MF barrier junctions are limited by the scarcity of existing single-phase multiferroics, and none of which combine large and robust electric and magnetic polarizations at room temperature. It might be a good idea to use a FE/FM composite barrier to substitute the single-phase MF barrier(41). Such a composite barrier junction may be thought as an addition of a conventional spin filter and a FTJ. Here, FM insulator (FI) barrier acts as a SF generator, and FE barrier acts as a SF adjustor through the interplay between ferroelectricity and ferromagnetism at the interface. The large SF effect, the TMR and TER effects, can be achieved in this two-phase composite barrier based tunnel junction. The eight resistive states with large difference can also be realized.
Electrostatic effect. Figure 23 shows a junction in which a FE/FI composite barrier is sandwiched by two metallic electrodes(41). The electrostatic potential induced by the electric polarization in FE layer is obtained, as shown in Fig. 23(b). The overall potential profile $U(x)$ across the junction is the superposition of the electrostatic potential $\varphi(x)$, the electronic potential in the electrodes, and the rectangular potential in FE barrier and FI barrier, as shown in Fig. 23(c).

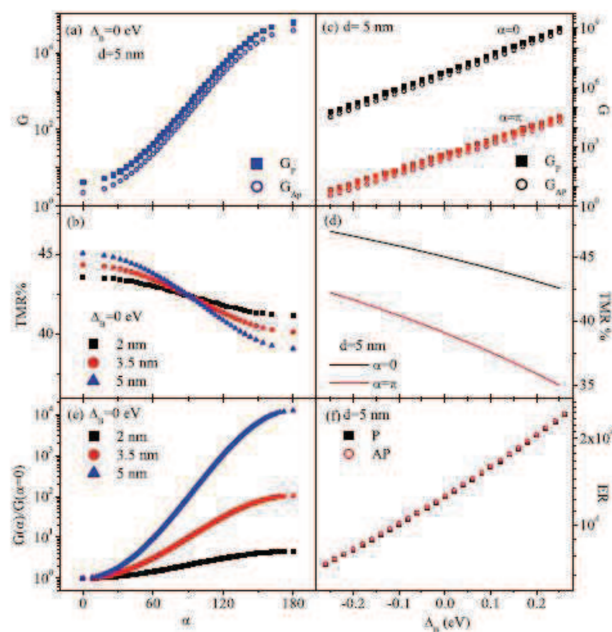

Fig. 20. (Color online) (a) The orientation of electric polarization α dependence of conductance. (b) dependence of TMR. (c) The exchange splitting of the barrier Δ_B vs conductance. (d) Δ_B vs TMR. (e) Δ_B dependence of the normalized conductance $G\alpha/G(\alpha=0)$ with parallel magnetization in two electrodes. (f) Δ_B dependence of TER with parallel (P) and antiparallel (AP) magnetizations in two electrodes(37).

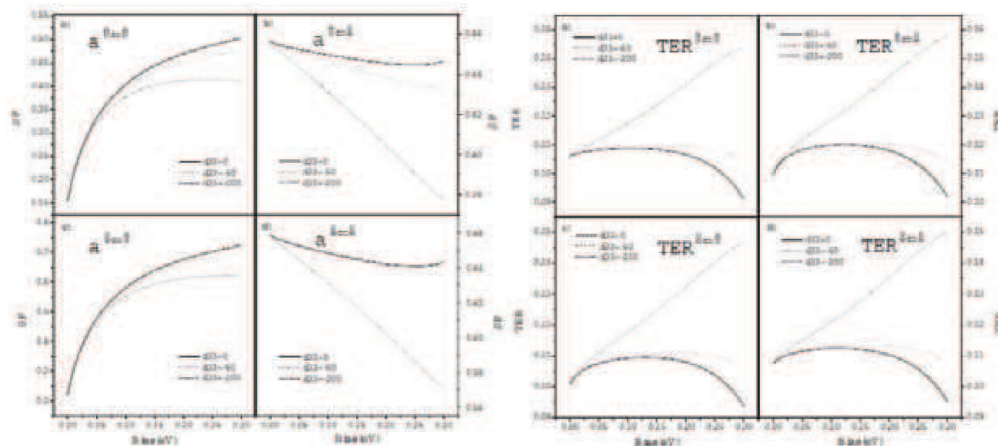

Fig. 21. (left panel)Piezoelectric effect on the SF and (right panel) TER(40) with Δ_B=0.015 eV, P=0.5 C/m^2, κ_3=-4.5 eV, μ_{33}=10, and Δ_L=Δ_R=0 eV.

Spin filtering effect, TMR and TER effect. Choosing the nonmagnetic metals (NMs) as two electrodes, the spin filtering efficiency can be defined as $\alpha = (G_{\uparrow} - G_{\downarrow})/(G_{\uparrow} + G_{\downarrow})$, while the TMR is defined by TMR=$(G_P - G_{AP})/(G_P + G_{AP})$ with changing the two metallic electrodes

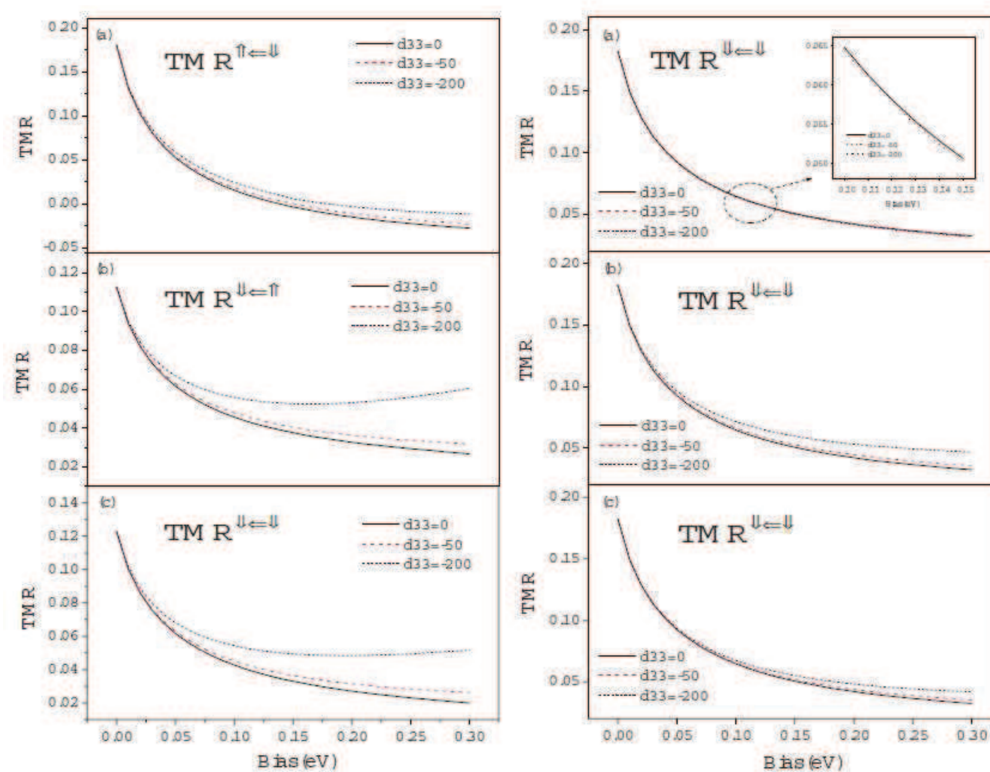

Fig. 22. (left panel)Piezoelectric effect on the TMR when Δ_B=0.015 eV, P=0.5 C/m^2, κ_3=-4.5 eV, μ_{33}=10, and Δ_L=0.05 eV, and Δ_R =0.09 eV. (right panel) Influence of only the (a) strain-induced barrier thickness change, (b) electron effective mass change, or (c) barrier height change on TMR. The inset in (a) shows the magnified curve around V=0.12 eV. The parameters are Δ_B=0.015 eV, P=0.5 C/m^2, Δ_L=0.05 eV, and Δ_R =0.09 eV(40).

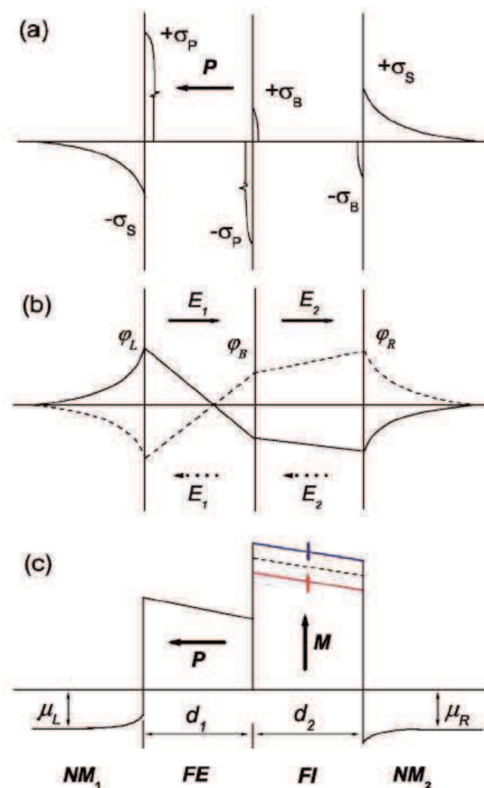

Fig. 23. (Color online) Schematic illustration of the charge distribution (a), corresponding electrostatic potential (b), and potential profile in a NM1/FE/ FI/NM2 tunnel junction C(41). The solid and dashed lines in (b) show the potential for the polarization P in FE barrier pointing to the left and to the right, respectively. The blue and red lines in FI barrier in (c) show the potential seen by the spin-down and spin-up electrons, respectively. Here d_1 and d_2 are the thicknesses of the FE and FI barriers, respectively.

from NMs to FM metals. To calculate TER, the direction of polarization in FE layer is reversed from pointing to the right to pointing to the left, while the magnetization in FI layer remains unchanged.

It can be seen from Fig. 24 that the SF and the TMR effect is mainly determined by the exchange splitting Δ_B in FI barrier, and is enhanced (reduced) by the polarization in FE barrier when P points the left (right) electrode. The results here are similar to those for the single-phase MF barrier junction, indicating that the physical mechanism responsible for SF effect is the same in both structures, i.e., the ferromagnetism in the barrier, making the barrier height spin dependent, acts as a SF generator, and the ferroelectricity, changing the profile of the potential across the junction, acts as a SF adjustor. A large TER effect can be found in MFTJs with composite barriers. The ferroelectricity in FE layer is the dominant factor to determine the magnitude of the TER effect.

Eight Logic states. By using one or two FM metal electrodes, eight independent logic states of tunneling conductance can be realized in such MFTJs. The conductances as a function of the exchange splitting Δ_B and the electric polarization P are shown in Fig. 24. For practical applications, the large contrast between eight states is very important. We find that when the carriers tunneling into the right electrode can be highly spin-polarized, the eight states are differentiated evidently.

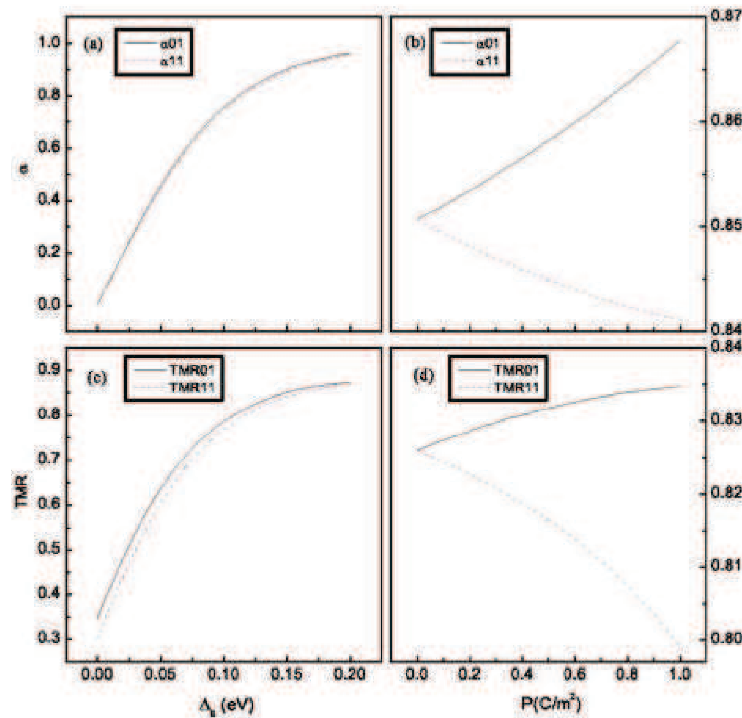

Fig. 24. (Color online) (a) The exchange splitting dependence of SF with P=0.4 C/m^2. (b) The electric polarization dependence of SF with Δ_B =0.13 eV. In (a) and (b), U_{01}=0.5 eV, U_{02}=1.1 eV, ε_{B1}=2000, ε_{B2}=1000, and d_1=d_2=2 nm. (c) and (d) show the corresponding TMR(41).

5. Magnetoelectric coupling at ferroelectrics/ferromagnetic metal interfaces

MFTJs have a great potential on the practical applications especially on the multistate logical elements. Due to the magnetoelectric coupling in MFTJ, it is perspective that the magnetization can be controled by the applied electric field, and vice versa. For single-phase multiferroic barrier, how the ferromagnetic order and ferroelectric order coupling is still a unsolved question. Therefore, we switch our attention to the ME coupling of the FM/FE/NM structures(Fig.26)(42).

Electrostatic effect at Ferromagnetic Metal / Ferroelectrics interfaces. For a FM/FE structure, when the FE layer is polarized, surface charges are created. These bound charges are compensated by the screening charge in both FM and NM electrodes. In the FM metal, the screening charges are spin polarized due to the ferromagnetic exchange interaction. The spin dependence of screening leads to additional magnetization in the FM electrode as illustrated in Fig. 26(b). If the density of screening charges is denoted as η and the spin polarization of screening charges is denoted as ζ, we can directly express the induced magnetization per unit area as

$$\Delta M = \frac{\eta}{e}\zeta\mu_B. \tag{10}$$

As this effect depends on the orientation of the electric polarization in FE, the ME coupling is expected.

Two simple cases can be considered. (1) In an ideal capacitor where all the surface charges reside at the metal (FM or NM)/FE interfaces, the density of screening charge η reaches its maximum value $\eta = P_0$, where P_0 is the spontaneous polarization of the FE. This results in a large induced magnetization $[(P_0/e)\zeta\mu_B]$. (2) In half metals, there is only one type of carriers that can provide the screening. If a half metal is chosen to be the FM electrode, the screening

electrons will be completely spin polarized. In this case, a large induced magnetization is also expected, $\Delta M = \frac{\eta}{e}\mu_B$.

Induced magnetization from screening charges. For FM/FE/NM junctions (Fig.26(a)), the additional magnetization, caused by spin-dependent screening(43)(44), will accumulate at each FM/FE interface. Due to the broken inversion symmetry between the FM/FE and the NM/FE interfaces, there would be a net additional magnetization in each FM/FE/NM unit cell, unlike the symmetric structures discussed in the previous work. The addition of magnetization in this superlattice will result in a large global magnetization. In the case of zero bias in Fig. 26(c), the local induced magnetization, defined as $\delta M(x) = [\delta n^{\uparrow}(x) - \delta n^{\downarrow}(x)]\mu_B$, is a function of distance from the interface x. Here, $\delta n^{\sigma}(x)$ is the density of the induced screening charges with spin σ. The total induced magnetization ΔM can be calculated by integrating $\delta M(x)$ over the FM layer, and

$$\Delta M = \int_{FM \quad layer} \delta M(x) = -\frac{\eta M_0/e}{N_0 + JN_0^2 - J(M_0/\mu_B)^2} \tag{11}$$

where $N_0 = N_{\uparrow} + N_{\downarrow}$ is the total density of states, $M_0 = (N_{\uparrow} - N_{\downarrow})\mu_B$ can be thought of as the spontaneous magnetization, ε_0 is the vacuum dielectric constant, J is the

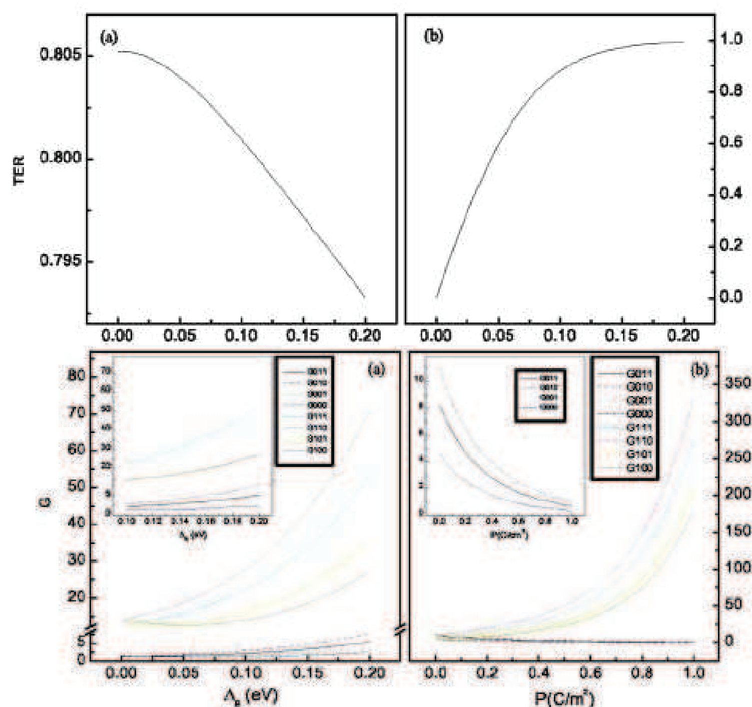

Fig. 25. (up panel) (a)The exchange splitting dependence of TER with P=0.4 C/m^2. (b) The electric polarization dependence of TER with Δ_B =0.13 eV. In (a) and (b), U_{01}=0.5 eV, U_{02}=1.1 eV, ε_{B1}=2000, ε_{B2}=1000, and d_1=d_2=2 nm. (down panel) (a) The exchange splitting and electric polarization dependence of tunneling conductances with P=0.4 C/m^2 in (a) and Δ_B =0.13 eV in (b)(41). In (a) and (b), the rectangular potential in FE barrier and FI barrier is 0.5 eV and 1.1 eV, respectively. ε_{B1}=2000, ε_{B2}=1000, and d_1=d_2=2 nm. The inset in (a) shows the enlarged part with Δ_B=0.1 eV. The inset in (b) shows the tunneling conductances with the polarization in FE barrier pointing to the left.

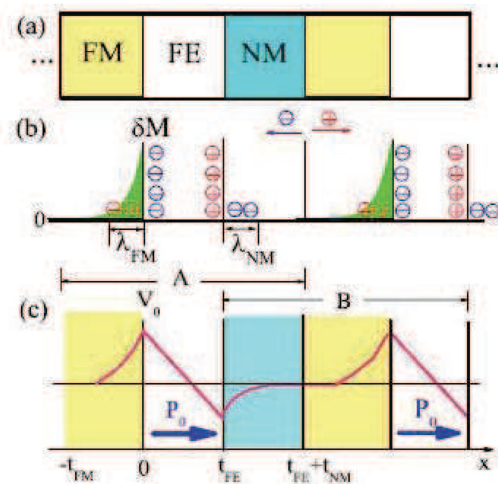

Fig. 26. (Color online) (a) Schematic illustration of FM/FE/NM tricomponent superlattice. (b) The distribution of charges and induced magnetization (green shaded area) calculated by our theoretical model. A and B are two different choices of the unit cell. The directions of arrows indicate the motions of positive and negative charges across the boundary of the unit cell A. (c) Electrostatic potential profile(42) . Here, the following assumptions are made. (1) The difference in the work function between FM and NM is ignored. (2) To screen the bound charges in FE, the charges in metal electrodes will accumulate at the FM/FE side, and there is a depletion at the NM/FE side. In this process, the total amount of charge is conserved; however, the spin density is not conserved because of the ferromagnetic exchange interaction in the FM metal.

strength of the ferromagnetic exchange coupling in the FM layer, η is the density of screening charges, $\lambda_{FM(NM)}$ is the screening length of FM (NM) electrode with $\lambda_{FM} = (e^2 N_0/\varepsilon_0)[N_0 + JN_0^2 - J(M_0/\mu_B)^2]/(1+JN_0)^{-1/2}$, and t_{FM}, t_{FE}, and t_{NM} are the thicknesses of FM, FE, and NM layers, respectively. It is seen that the local induced magnetization $\delta M(x)$ decays exponentially away from the FM/FE interface.

The induced magnetization in FM/FE/NM tricomponent superlattice with several FM electrodes, i.e., Fe, Co, Ni, and CrO_2, are calculated.(42) Detailed parameters and calculated values of Δ_M are listed in Fig.27. The magnitude of Δ_M is found to depend strongly on the choice of the FM and FE. Among the normal FM metals (Ni, Co, and Fe), the largest Δ_M is observed in Ni for its smallest J and highest spontaneous spin polarization $M_0/\mu_B N_0$. On the other hand, we also predict a large Δ_M for the 100% spontaneous spin polarization in half-metallic CrO_2.

FM	J (eV nm^3)	N_0 (eV^{-1} nm^{-3})	$M_0/\mu_B N_0$ (%)	λ_{FM} (Å)	ΔM (μ_B nm^{-2})	τ (G cm/V)
Ni	0.65	1.74	−79.3	0.9	−0.280	0.015
Co	1.25	0.89	−58.4	1.5	−0.126	0.004
Fe	2.40	1.11	56.8	1.3	0.078	0.003
CrO_2	1.8	0.69	100	1.7	0.323	0.010

Fig. 27. Calculated induced magnetization(42). Here, ΔM is the value at V_a=V_C, where V_a is the applied bias and V_C is the coercive bias.

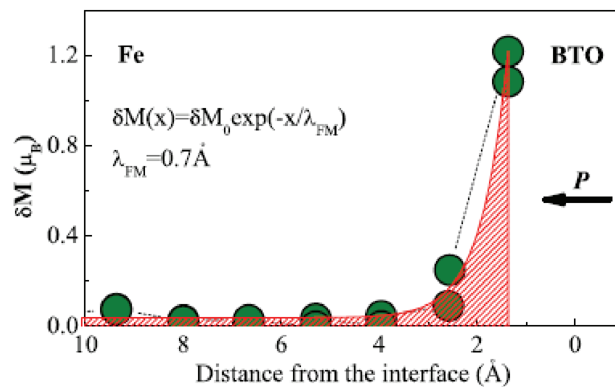

Fig. 28. (Color online) Layer-resolved induced magnetic moment of Fe near the interface between Fe and $BaTiO_3$ in the Fe/$BaTiO_3$ / Pt superlattice(42). Solid line is the fitted exponential function for the induced moment as a function of the distance from the interface.

First-principle calculations. The first-principle calculations are consistent with the results of the theoretical model. For example, the first-principle calculation of the Fe/FE/Pt superlattice will be shown.(45) The calculations are within the local-density approximation to density-functional theory and are carried out with VASP. We choose $BaTiO_3$ (BTO) and $PbTiO_3$ (PTO) for the FE layer. Starting from the ferroelectric P4mm phase of BTO and PTO with polarization pointing along the superlattice stacking direction, we perform a structural optimization of the multilayer structures by minimizing their total energies. The in-plane lattice constants are fixed to those of the tetragonal phase of bulk FEs. Figure 19 shows the calculated induced magnetic moment relative to that of bulk Fe near the Fe/BTO interface when the polarization in $BaTiO_3$ points toward the Fe/BTO interface. It is evident that the induced moments decay exponentially as the distance from the interface increases. This result is in line with our model for the magnetization accumulation in the FM at the FM/FE interface. A numerical fitting of the exponential function yields a screening length of 0.7 Åfor the Fe/$BaTiO_3$ / Pt structure. This value is comparable to the screening length parameters calculated using the theoretical model as shown in Fig.28.

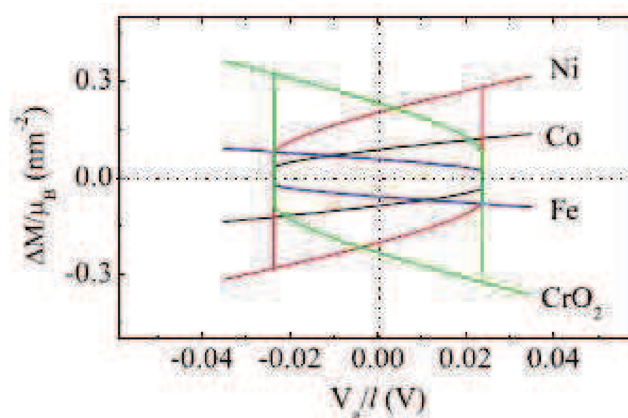

Fig. 29. (Color online) ΔM versus V_a/l for different ferromagnetic metal electrodes. V_a is the applied bias and l is the number of the unit cell(42). Here, the thickness of FE layer is 3 nm. However, a thicker FE layer can be used to avoid the possible electron tunneling effect.

Electric Control of Magnetization. A natural question is what happens to Δ_M when an external bias V is applied. In this case, the electric polarization P will have two parts: the spontaneous polarization P_0 and the induced polarization. The equation determining P is obtained by minimizing the free energy. From the continuity of the normal component of the electric displacement, we find equation relating η and P:$\eta = [(Pt_{FE}/\varepsilon_{FE}) + (V_a/l)]/[(\lambda_{FM} + \lambda_{NM})/\varepsilon_0] + (t_{FE}/\varepsilon_B)$. Here, ε_{FE} is the dielectric constant of the FE layer. These two equations need to be solved self-consistently. The value of η at a given bias can then be calculated and the induced magnetization ΔM is given by Eq. (11). The free-energy density F includes contributions from the FE layer, FM layer, and FM/FE interface and takes the form

$$F = \frac{t_{FE}F(P) + t_{FM}F(M) + F_I(F,M)}{t_{FE} + t_{FM} + t_{NM}} \tag{12}$$

M is the magnetization of the bulk ferromagnet and here $M = M_0$ because of zero external magnetic field. The interface energy $F_I(P,M)$ is the sum of the electrostatic energy and magnetic exchange energy of the screening charges,

$$F_I(F,M) = \frac{(\lambda_{FM} + \lambda_{NM})}{2\varepsilon_0}\eta^2 + \frac{J}{2\mu_B^2}(M + \Delta M)\Delta M \tag{13}$$

For FE, the free-energy density $F(P)$ can be expressed as $F(P) = F_P + \alpha_P P^2 + \beta_P P^4 + \int_0^P E_B dP$, where F_P is the freeenergy density in the unpolarized state. α_P and β_P are the usual Landau parameters of bulk ferroelectric. E_B is the depolarization field in the FE film. Similarly, $F(M)$ can be expanded as a series in the order parameter M, i.e., $F(M) = F_M + \mu_M M^2 + \nu_M M^4$, where F_M is the free-energy density of bulk ferromagnet and μ_M and ν_M are the Landau parameters of bulk ferromagnet. The calculated induced magnetization as a function of the applied bias is shown in Fig. 29. Clearly, the electrically controllable magnetization reversal is realized.

Magnetoelectric coupling energy at the FM/FE interface. To discuss the macroscopic properties of the electric control of magnetization, we analyze the magnetoelectric coupling energy in our tricomponent superlattice. For the macroscopic average polarization to be represented by the electric polarization obtained for a unit cell, this cell needs to be chosen with special care. Therefore, in the following calculation of total free energy, unit cell B in Fig. 26(b) is chosen, and

$$\bar{P} = \frac{Pt_{FE} + \eta\,(t_{FM} + t_{NM})}{t_{FE} + t_{FM} + t_{NM}} \tag{14}$$

The macroscopic average magnetization

$$\bar{M} = \frac{Mt_{FM} + \Delta M}{t_{FE} + t_{FM} + t_{NM}} \tag{15}$$

Considering the lowest-order term of the magnetoelectric coupling, $\bar{P}$ and $\bar{M}$ can be expanded as $\bar{P} = c_p P + c_p' PM^2$, $\bar{M} = c_m M + c_m' PM$. Therefore, the total free energy [Eq. (12)] can be expressed as the power series of $\bar{P}$ and $\bar{M}$, $F(\bar{P},\bar{M}) = F_0 + \alpha\bar{P}^2 + \beta\bar{P}^4 + \mu\bar{M}^2 + \nu\bar{M}^4 + \chi\bar{P}\bar{M}^2 + \cdots$. We would like to point out that biquadratic ME coupling $\bar{P}^2\bar{M}^2$ is easily achievable, but is usually weak and is not electrically controllable. However, because of the naturally broken inversion symmetry, the large ME coupling $\bar{P}\bar{M}^2$ is possible in our tricomponent structure.

6. Summary

Ferroelectric and multiferroic tunnel junctions have shown great promise for practical applications, i.e., high density data storage. However, to realize these junctions, a number of questions are required to be answered. For example, how the electric polarization switches in nanoscale ferroelectrics? How the ultrathin ferroelectric barrier change the magnetic and electric properties of electrode/barrier interfaces? How the ferroelectric domain affect the tunneling across FTJs and MFTJs? Nowadays, achievements in the field of complex oxide epitaxy and newly developed nanoscale characterization techniques, promise that the realization of FTJs and MFTJs is just a matter of time. The diversity of interesting physical phenomena that control the characteristics of these tunnel junctions and their multifunctional properties makes the research in this field challenging and promising.

7. Acknowledgments

This project was supported by the National Natural Science Foundation of China by grants No. 10774107 and No. 10974140.

8. References

[1] P. M. Tedrow, R. Meservey, Phys. Rev. Lett. 26, 192 (1971).
[2] P. M. Tedrow, R. Meservey, Phys. Rev. B 7, 318 (1973).
[3] M. Jullire, Phys. Lett. A 54, 225 (1975).
[4] J. S. Moodera *et al.*, Phys. Rev. Lett. 74, 3273 (1995).
[5] J. M. De Teresa *et al.*, Science 286, 507 (1999).
[6] S. Ikeda, J. Hayakawa, Y. Ashiizawa *et al.*, Appl. Phys. Lett. 93, 082508 (2008).
[7] W. H. Butler, X. G. Zhang, T. C. Schulthess, Phys. Rev. B 63, 054416 (2001).
[8] J. Mathon and A. Umersski, Phys. Rev. B 63, 220403(R) (2001).
[9] J. S. Moodera *et al.*, Phys. Rev. Lett. 61, 637 (1988).
[10] J. S. Moodera, R. Meservey, and X. Hao, Phys. Rev. Lett. 70, 853 (1993).
[11] T. S. Santos *et al.*, Phys. Rev. B 69, 241203 (2004).
[12] P. LeClair *et al.*, Appl. Phys. Lett. 80, 625 (2002).
[13] L. Esaki, R. B. Laibowitz, P. J. Stiles, IBM Tech. Discl. Bull. 13, 2161 (1971).
[14] M. Ye. Zhuravlev *et al.*, Phys. Rev. Lett. 94, 246802 (2005).
[15] E. Y. Tsymbal and H. Kohlstedt, Science 313, 181 (2006).
[16] A.V. Bune, V. M. Fridkin, S. Ducharme, L. M. Blinov, S. P. Palto, A.V. Sorokin, S. G. Yudin, and A. Zlatkin, Nature (London) 391, 874 (1998).
[17] D. D. Fong, G. B. Stephenson, S. K. Streiffer, J.A. Eastman, O. Auciello, P. H. Fuoss, and C. Thompson, Science 304, 1650 (2004).
[18] J. Junquera and P. Ghosez, Nature (London) 422, 506 (2003).
[19] N.W. Ashcroft and N. D. Mermin, Solid State Physics (Saunders College Publishing, New York, 1976), p. 340.
[20] C. B. Duke, Tunneling in Solids (Academic, New York, 1969).
[21] V. Garcia *et al.*, Nature 460, 81 (2009)
[22] A. Gruverman, Nano Letters 9, 3539 (2009)
[23] A. Crassous *et al.*, Appl. Phys. Lett. 96, 042901 (2010)
[24] P. Maksymovych *et al.*, Science 324, 1421 (2009)
[25] D. D. Fong *et al.*, Phys. Rev. B 71, 144112 (2005).
[26] G. Gerra *et al.*, Phys. Rev. Lett. 96, 107603 (2006).

[27] H. Kohlstedt *et al.*, Phys. Rev. B 72, 125341 (2005).
[28] M. Ye. Zhuravlev *et al.*, Appl. Phys. Lett. 95, 052902 (2009).
[29] Y. Wu, S. Ju, and Z. Y. Li, Appl. Phys. Lett. 96, 252905 (2010)
[30] M. Ye. Zhuravlev *et al.*, Appl. Phys. Lett. 87, 222114 (2009).
[31] V. Garcia et al., Science 327, 1106 (2010)
[32] M. Gajek *et al.*, Phys. Rev. B 72, 020406 (2005).
[33] H. Bèa *et al.*, Appl. Phys. Lett. 88, 062502 (2006)
[34] H. Bèa *et al.*, J. Phys. Condens. Matter 20, 434221 (2008).
[35] M. Gajek *et al.*, Nat. Mater. 6, 296 (2007).
[36] S. Ju *et al.*, Phys. Rev. B 75, 064419 (2007).
[37] S. Ju *et al.*, J. Appl. Phys. 104, 093504 (2008).
[38] D. F. Jin, Y. Ren, Z. Z. Li, M.W. Xiao, G. J. Jin, and A. Hu, Phys. Rev. B 73, 012414 (2006).
[39] J. C. Slonczewski, Phys. Rev. B 39, 6995 (1989)
[40] J. Wang, S. Ju, and Z. Y. Li, J. Appl. Phys. 105, 093920 (2009).
[41] J. Wang and Z. Y. Li, Appl. Phys. Lett. 93, 112501 (2008).
[42] T. Cai *et al.*, Phys. Rev. B 80, 140415(R) (2009)
[43] S. F. Zhang, Phys. Rev. Lett. 83, 640 (1999).
[44] J. M. Rondinelli, M. Stengel, and N. A. Spaldin, Nat. Nanotechnol. 3, 46 (2008).
[45] J. K. Lee, N. Sai, T. Y. Cai, Q. Niu, and A. A. Demkov, Phys. Rev. B 81, 144425 (2010).

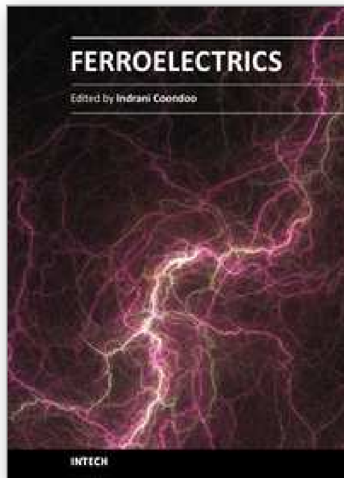

Ferroelectrics
Edited by Dr Indrani Coondoo

ISBN 978-953-307-439-9
Hard cover, 450 pages
Publisher InTech
Published online 14, December, 2010
Published in print edition December, 2010

Ferroelectric materials exhibit a wide spectrum of functional properties, including switchable polarization, piezoelectricity, high non-linear optical activity, pyroelectricity, and non-linear dielectric behaviour. These properties are crucial for application in electronic devices such as sensors, microactuators, infrared detectors, microwave phase filters and, non-volatile memories. This unique combination of properties of ferroelectric materials has attracted researchers and engineers for a long time. This book reviews a wide range of diverse topics related to the phenomenon of ferroelectricity (in the bulk as well as thin film form) and provides a forum for scientists, engineers, and students working in this field. The present book containing 24 chapters is a result of contributions of experts from international scientific community working in different aspects of ferroelectricity related to experimental and theoretical work aimed at the understanding of ferroelectricity and their utilization in devices. It provides an up-to-date insightful coverage to the recent advances in the synthesis, characterization, functional properties and potential device applications in specialized areas.

How to reference
In order to correctly reference this scholarly work, feel free to copy and paste the following:

Tianyi Cai, Sheng Ju, Jian Wang and Zhen-Ya Li (2010). Ferroelectric and Multiferroic Tunnel Junctions, Ferroelectrics, Dr Indrani Coondoo (Ed.), ISBN: 978-953-307-439-9, InTech, Available from: http://www.intechopen.com/books/ferroelectrics/tunneling-electroresistance-and-magnetoresistance-in-ferroelectrics-based-tunneling-junctions

INTECH
open science | open minds

InTech Europe
University Campus STeP Ri
Slavka Krautzeka 83/A
51000 Rijeka, Croatia
Phone: +385 (51) 770 447
Fax: +385 (51) 686 166
www.intechopen.com

InTech China
Unit 405, Office Block, Hotel Equatorial Shanghai
No.65, Yan An Road (West), Shanghai, 200040, China
中国上海市延安西路65号上海国际贵都大饭店办公楼405单元
Phone: +86-21-62489820
Fax: +86-21-62489821

© 2010 The Author(s). Licensee IntechOpen. This chapter is distributed under the terms of the Creative Commons Attribution-NonCommercial-ShareAlike-3.0 License, which permits use, distribution and reproduction for non-commercial purposes, provided the original is properly cited and derivative works building on this content are distributed under the same license.